A Model of the Interaction between N-type and C-type Inactivation in Kv1.4 Channels

Glenna C. L. Bett,[†‡§] Isidore Dinga-Madou,[‡§] Qinlian Zhou,[‡§] Vladimir E. Bondarenko,[‡§] and Randall L. Rasmusson[‡§*]

[†]Departments of Gynecology-Obstetrics and [‡]Physiology and Biophysics, The State University of New York, University at Buffalo, Buffalo, New York; and [§]Center for Cellular and Systems Electrophysiology, School of Medicine & Biomedical Sciences, Buffalo, New York

ABSTRACT Kv1.4 channels are *Shaker*-related voltage-gated potassium channels with two distinct inactivation mechanisms. Fast N-type inactivation operates by a ball-and-chain mechanism. Slower C-type inactivation is not so well defined, but involves intracellular and extracellular conformational changes of the channel. We studied the interaction between inactivation mechanisms using two-electrode voltage-clamp of Kv1.4 and Kv1.4ΔN (amino acids 2–146 deleted to remove N-type inactivation) heterologously expressed in *Xenopus* oocytes. We manipulated C-type inactivation by introducing a lysine-tyrosine point mutation (K532Y, equivalent to *Shaker* T449Y) that diminishes C-type inactivation. We used experimental data to develop a comprehensive computer model of Kv1.4 channels to determine the interaction between activation and N- and C-type inactivation mechanisms needed to replicate the experimental data. C-type inactivation began at lower voltage preactivated states, whereas N-type inactivation was coupled directly to the open state. A model with distinct N- and C-type inactivated states was not able to reproduce experimental data, and direct transitions between N- and C-type inactivated states were required, i.e., there is coupling between N- and C-type inactivated states. C-type inactivation is the rate-limiting step determining recovery from inactivation, so understanding C-type inactivation, and how it is coupled to N-type inactivation, is critical in understanding how channels act to repetitive stimulation.

INTRODUCTION

KCNA4 encodes the α-subunit of the voltage-gated K^+ channel, Kv1.4, a member of the *Shaker*-related family. Depolarization of Kv1.4 channels produces a rapidly activating and inactivating transient current with a relatively slow recovery from inactivation. Kv1.4 channels have been found in diverse cell types including smooth muscle (1), neurons (2–4), and the heart (5–7). The rapid and short-lived Kv1.4 current is called A-type in neurons, and is transient outward in the heart. Kv1.4 expression is upregulated in hypertrophy and heart failure (8–10).

Inactivation of Kv1.4 channels is complex, involving at least two distinct mechanisms: N- and C-type. N-type inactivation is the result of rapid block of the conducting pore by the lipophilic N-terminal region of the channel, after channel opening (11–13). Binding of the N-terminal to the fully open channel is voltage-insensitive (11,14) and reflects coupling of the N-terminal to channel opening. C-type inactivation in the absence of the N-terminal domain in Kv1.4 is also voltage-insensitive and reflects a coupling to channel activation (14), despite occurring through a very different mechanism involving closure or collapse of the permeation pathway at both the intracellular and extracellular mouth of the pore (15).

In addition to being coupled to the process of activation, N- and C-type inactivations are coupled to each other (16,17). The development of N-type inactivation drives the channel quickly into a C-type inactivated state (16–19) and this combined N- and C-type inactivated state governs recovery from inactivation, giving it the properties of recovery from C-type inactivation (16,17). In this study, we quantitatively examine the nature of this coupling, and the relative degree of activation required to allow both N- and C-type inactivation to develop. Experiments were performed on Kv1.4 (with both N- and C-type inactivation), Kv1.4ΔN (amino acids 2–146 are deleted to remove N-type inactivation), and Kv1.4[K532Y] (which has N-type inactivation but limited C-type inactivation) (17). This mutation is equivalent to T449Y in *Shaker* (20). Data were used to develop a computer model of the coupling of activation to inactivation and the coupling between N- and C-type inactivation in Kv1.4.

METHODS

Electrophysiology

Oocytes were prepared as described in Bett and Rasmusson (21). *Xenopus laevis* (*Xenopus* Express) were cared for by standards approved by the Institutional Animal Care and Use Committee of the University at Buffalo. Frogs were anesthetized (1 g/L tricaine solution; Sigma, St. Louis, MO), and oocytes placed in OR2 (82.5 mM NaCl, 2 mM KCl, 1 mM $MgCl_2$, 5 mM HEPES; pH 7.4, 1 mg mL^{-1} collagenase, type I; Sigma) for 1.5–2 h. Defolliculated oocytes (stage V-VI) were injected with up to 50 ng mRNA via Nanoject microinjection (Drummond Scientific, Broomall, PA).

Molecular biology

The cDNA constructs for ferret Kv1.4 (fKv1.4), used in this study (i.e., fKv1.4ΔN and fKv1.4[K532Y]), have been previously described (17,22).

Submitted July 27, 2010, and accepted for publication November 8, 2010.

*Correspondence: rr32@buffalo.edu

Editor: Michael Pusch.

0006-3495/11/01/0011/11 $2.00

doi: 10.1016/j.bpj.2010.11.011

Removal of residues 2–146 (N-terminal domain, ΔN) results in a loss of N- but leaves C-type inactivation. Mutation K532Y markedly slows C-type inactivation (17). Mutations were made using QuikChange (Stratagene, La Jolla, CA). A schematic diagram of the mutants and constructs used are shown in Fig. 1 *A*.

Oocytes were voltage-clamped in whole-cell configuration using a two-electrode oocyte clamp amplifier (CA-1B; Dagan, Minneapolis, MN), at room temperature. Microelectrodes (0.5–1.5 MΩ, filled with 3 M KCl) were fabricated from 1.5 mm o.d. borosilicate glass (TW150-4; WPI, Sarasota, FL) using a two-stage puller (David Kopf Instruments, Tujunga, FL). Extracellular solution (2 mM K^+) contained: 96 mM NaCl, 2 mM KCl, 1 mM $MgCl_2$, 1.8 mM $CaCl_2$, 10 mM HEPES, pH 7.4. Voltage-clamp protocols are described as appropriate in the text. The holding potential and the interpulse potential for recovery measurements was −90 mV, unless otherwise noted.

Data analysis

Data were filtered at 2 kHz, digitized and analyzed using pCLAMP 9.2 (Molecular Devices, Eugene, OR). Further analysis was performed using Clampfit (Molecular Devices), Excel (Microsoft, Redmond, WA) and Origin (Microcal, Northampton, MA). Data are shown as mean ± SE.

Computer modeling

Programs were written in Visual Basic (Visual Studio.Net) on a Dell Optiplex GX260 and in Microsoft Visual C++ 2008 on a Dell Precision T7500 with two Intel Xeon CPU E5520s. Channel gating was modeled as discrete transitions between Markov states. All differential equations were numerically solved by implementation of a fourth-order Runge-Kutta method. All simulations were tested for insensitivity to time step size to ensure accuracy of numerical integration. All kinetic equations were constrained to produce detailed thermodynamic reversibility.

Open Kv1.4 channels were assumed to act as linear Ohmic conductors of current,

$$I = \gamma P_o(E - E_{rev}), \quad (1)$$

where I is whole-cell current, γ is whole-cell conductance, P_o is the probability of the channel being in the open state, E_{rev} is the reversal potential, and E is membrane potential. The Kv1.4 ion transfer relation (conductance) is nonlinear, and exhibits slight outward rectification, which is absent from model, hence the slight difference in simulated versus experimental IV curves. These curves were not used to derive the model, and no attempt was made to fit them. All experimental protocols were designed to avoid this complication in analysis, i.e., G/G_{max} curves were not used. There is a slight discrepancy at the foot of the pseudo-steady-state activation curve which reflects a slight limitation of the gating model fitting and is not related to the non-Ohmic properties of the open channel. A simplified Ohmic conductance was assumed for simplicity in generating curves that resembled experimentally obtained data. Kv1.4 [K532Y] has a different relationship between $[K^+]_o$ and conductance, which could conceivably cause changes in outward rectification. This would require two analyses and two models, further complicating analysis but without affecting the focus of our work, which is the relationship between inactivated states. The final rate constants used in the model are given in Table 1.

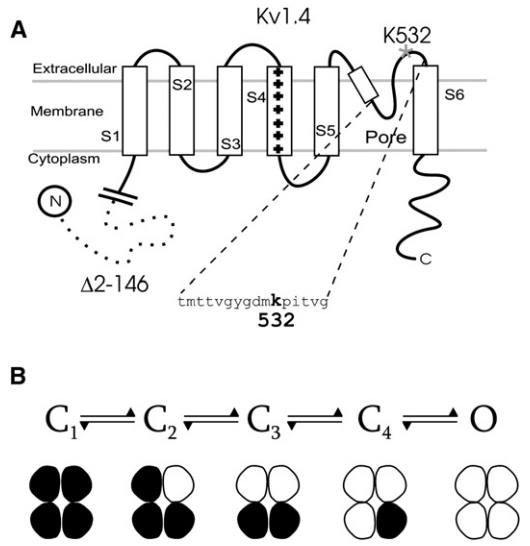

FIGURE 1 (*A*) Schematic representation of the Kv1.4 channel constructs used in this study. Kv1.4 is a typical voltage-gated channel with six transmembrane-spanning domains, one of which (S4) is charged and thought to be the voltage sensor. The N-terminal forms a ball and chain which can occlude the open channel. In the ΔN construct, amino acids 2–146 are deleted, removing the N-terminal and thus N-type inactivation. A lysine-to-tyrosine point mutation on the extracellular side of S6 was made (Kv1.4[K532Y]). This mutation drastically reduces the ability of the channel to undergo C-type inactivation. (*B*) Activation requires multiple closed states to reproduce the sigmoid onset of activation. Kv1.4 channels are tetramers, so we modeled the channel with four closed states. All transitions in the Markov model therefore correspond to the activation of one of the four subunits which form the basic core of the channel. The channel is only open, i.e., passes current, when all four subunits are activated.

Determination of parameter values and rejection of alternatives

Most parameters were determined algebraically and were highly constrained by experimental data. Parameters for the activation model were extracted algebraically from the equations reported as nonlinear least-squares best fits to data in Comer et al. (22). K_{fc} and K_{bc} (C-type inactivation) were estimated using Kv1.4ΔN, in which the time constant for inactivation is

$$1/(K_{fc} + K_{bc}).$$

K_{fc} and K_{bc} were set to produce a good match to the average data. K_{bc} was initially determined from the degree of inactivation at 5 s adjusted to steady state by $e^{-5/tau}$. Parameters were systematically varied to demonstrate that no solution could give a recovery ($1/K_{bc}$) consistent with the forward rate of inactivation, the degree of inactivation at 5 s, and recovery rate.

A solution that matched both the degree of inactivation at 5 s and forward rate of recovery were chosen for the final parameters. This yields a value for $1/K_{bc}$ that was almost exactly twice as slow as the recovery rate, hence the factor of 2 for the backward rate from inactivation to the preactivated closed state. Equal factors for all K_{bc} could be ruled out algebraically, as there is no combination of K_{bc} and K_{fc} that was within the standard errors for the time

TABLE 1 Values of rate constants used in the program

Rate	Value (s^{-1})
K_{fc}	0.2443
K_{bc}	0.1514
K_{fn}	14.2429
K_{bn}	1.4818
K_{f1}	3.2612
K_{b1}	0.5067
K_{f2}	4.6816
K_{b2}	$K_{f2}*K_{b1}*K_{fc}*K_{bn}/(K_{bc}*K_{fn}*K_{f1})$

constant of inactivation and ±5 SE inactivation relationship and which also reasonably reproduced recovery. K_{fN} and K_{bN} (N-type inactivation) were estimated directly from best fits of the time constant for inactivation ($1/(K_{fN}+K_{bN})$) and the nonlinear least-squares estimate of time constant of recovery from N-type inactivation in Kv1.4[K532Y] ($1/K_{bN}$). As an additional constraint, they were checked to ensure the residual noninactivating component was indistinguishable from leak and background currents. Rejection of models for the degree of coupling used the same well-constrained states for all situations. We examined the ability of changes in rate constants to shift $V_{1/2}$. Large shifts in $V_{1/2}$ of inactivation required changes in K_b and K_f that were out of the range of experimental observations.

RESULTS

Activation

The model of activation was developed from the previously published activation kinetics of Comer et al. (22). Kv1.4 channel activation is clearly a sigmoidal process, which suggests that the channel transitions through multiple closed states before opening. Kinetic data from Hoshi et al. (11) were fit to a Hodgkin- Huxley (23) process, with an equation of the form

$$\left(1-\exp\left(-\frac{t}{\tau_a}\right)\right)^n, \tag{2}$$

where t = time, τ_a = time constant of activation, and n = activation power. Data were well fit when $n = 4$, so activation was modeled as a four-state Markovian process, with four independently gating units and corresponding to the cartoon of a tetramer of α-subunits, as shown in Fig. 1 *B*. The fits to the steady-state and kinetic activation data from Comer et al. (22) were transformed algebraically from the form

$$P_{open} = \frac{1}{\left(1+\frac{\beta}{\alpha}\right)}, \tag{3}$$

$$\tau = \frac{1}{\alpha+\beta}, \tag{4}$$

to voltage-dependent forward (α) and backward (β) rate constants determined by the following equations:

$$\alpha = 950\exp\left(\frac{V-40.4}{49.2}\right), \tag{5}$$

$$\beta = 617.5\exp\left(\frac{V-40.4}{49.2}\right)\left(\frac{\exp\left(-\frac{V+48.4}{13.6}\right)}{1+0.004\exp\left(-\frac{V+48.4}{13.6}\right)}\right). \tag{6}$$

Fig. 2 *A* shows the normalized peak I/V relationship for Kv1.4ΔN. At positive potentials the probability of the channels being open, P_o, is assumed to be 1, and the whole cell conductance, γ, was determined from the slope of the line using Eq. 1. Fig. 2 also shows experimental data from Comer et al. (22), used to calculate activation rate constants. Fig. 2 *B* shows Tau activation versus voltage, and Fig. 2 *C* shows steady-state activation. These data indicate that the approximations in the analysis of the time and voltage

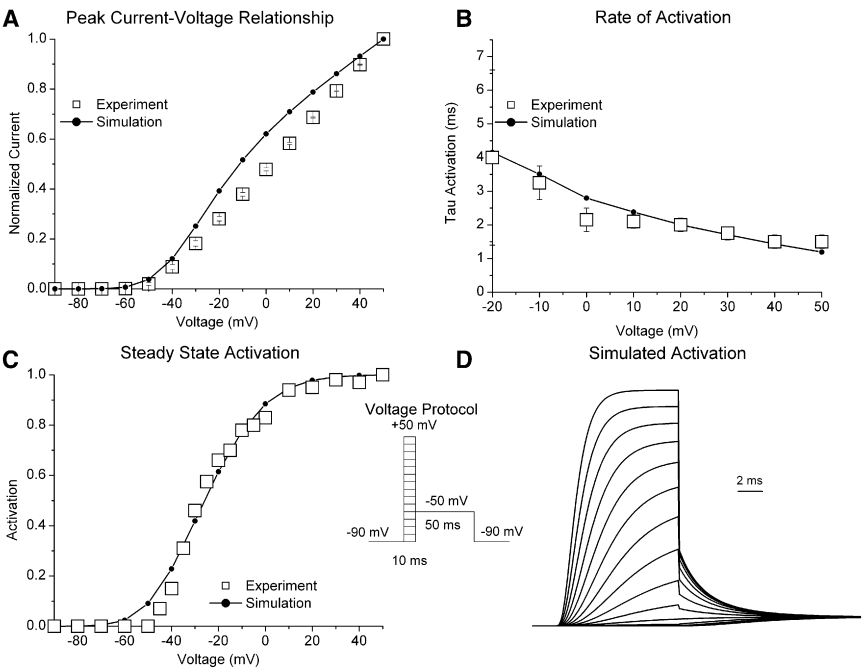

FIGURE 2 Activation of Kv1.4 channels. (*A*) Peak I/V relationship from Kv1.4 ΔN. From a potential of −90 mV, oocytes were depolarized to potentials from −90 to + 50 mV. Experiment (□, $n = 10$) and simulation (●). (*B*) Rate of activation. Experiment (□, from Comer et al. (22) and simulation (●). (*C*) Steady-state activation was determined using the voltage protocol. (*Inset*) A 10-ms depolarizing step (P1) to potentials between −90 and +50 mV was followed by a (P2) step to −50 mV. Experiment (□, from Comer et al. (22)), and simulation (●). (*D*) Simulated current traces using the voltage protocol shown in the inset.

dependence of the rate of activation enabled reproduction of the time- and voltage-dependence of activation. Simulated current traces are shown in Fig. 2 *D*.

C-type inactivation

Kv1.4 channels possess two types of inactivation: N- and C-type. N-type inactivation is the result of pore occlusion after binding of the N-terminal ball to sites on the intracellular pore mouth, and can be removed by deleting the N-terminal. We studied the N-terminal deleted construct, Kv1.4ΔN, which has C-type inactivation in the absence of N-type inactivation. We tested four models of coupling between C-type inactivation and the activation model:

Model C1

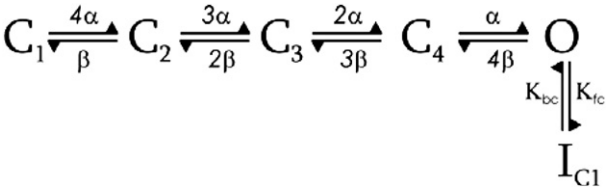

Model C2

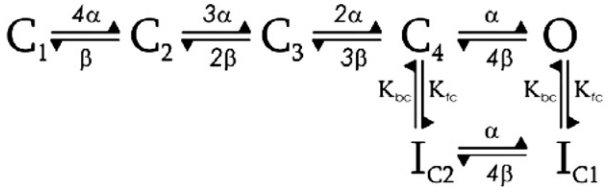

Model C3

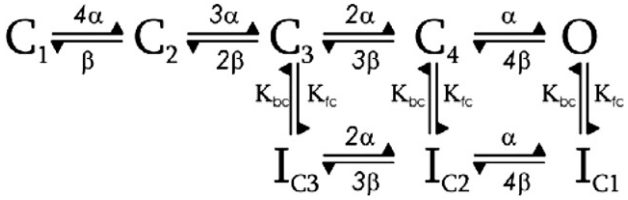

Model C4

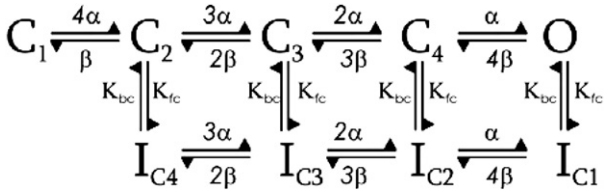

Rate constants for the development of C-type inactivation were set to be voltage insensitive to be consistent with experimental observation of the voltage insensitivity of this process. The ability of each model to simulate Kv1.4ΔN isochronal inactivation was tested with K_{bc} and K_{fc} adjusted to match the rate and degree of inactivation developed during the test pulse. If the C-type inactivated state (I_C) can only be accessed through the open state, the degree of inactivation is always significantly less than the experimentally observed value over the range –50 to –20 mV (Fig. 3). The experimental data can only be reproduced by the introduction of transitions between the first preactivated closed state and I_C. Fig. 3 *A* shows that simulations using model C2 best fit the experimental data, so this model was used as basic model of C-type inactivation coupled to activation. Fig. 3 *B* shows the simulated current from model C2 in response to a standard two-pulse protocol.

Recovery from inactivation is dominated by recovery from the C-type inactivated state, regardless of whether the N-type inactivation is present. We used a variable interval two-pulse protocol to determine the rate of recovery from C-type inactivation. Fig. 3 *C* shows that recovery from inactivation could not be reproduced with model C2. Even though the rate of recovery was slow, the transition from I_{C2} to C_4 could not be made fast enough if K_{bc} was set to be uniform from I_{C1} and I_{C2}. However, if the transition from I_{C2} to C_4 was set to $2K_{bc}$ (the transition from I_{C1} to O) with a corresponding reduction in the transition from I_{C1} to I_{C2} from 4β to 2β to maintain thermodynamic reversibility, the experimental data were reproduced:

Model C2a

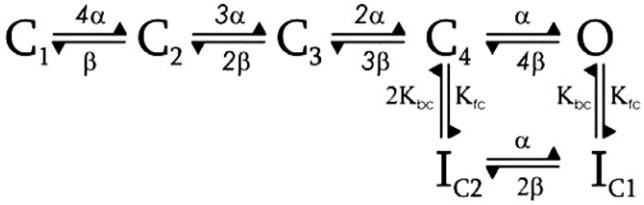

The introduction of C-type inactivation did not have a great impact on the activation properties of the model, i.e., peak IV and isochronal activation, which were well matched to the experimental data of Comer et al. (22) (see the Supporting Material). C-type inactivation is well fit by a single exponential, and Fig. 4 shows that it is voltage-independent at potentials where activation is complete.

N-type inactivation

N- and C-type inactivation coexists in Kv1.4 channels. Although C-type inactivation involves significant movement of both the intracellular and extracellular pore, and is not confined to a single deletable region of the channel, the development of C-type inactivation is severely restricted when a lysine residue (K532) at the outer edge of S6 is mutated to tyrosine. We studied the behavior of Kv1.4 [K532Y] channels, which have N-type, but lack C-type inactivation, to develop a model of N-type inactivation coupled to the activation model. We tested the ability of

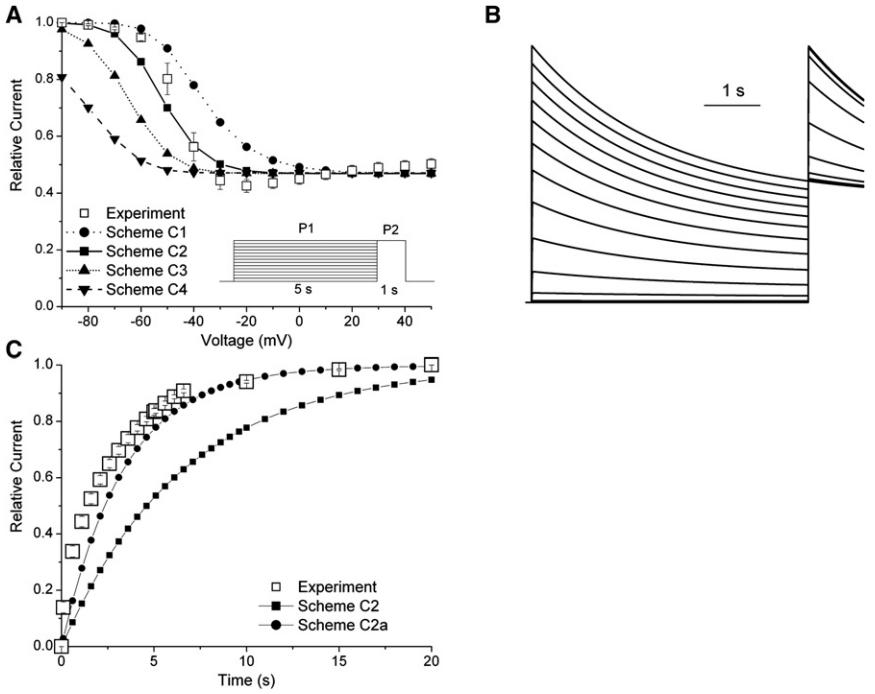

FIGURE 3 Coupling C-type Isochronal inactivation to activation in Kv1.4ΔN. A standard two-pulse protocol was used to measure isochronal inactivation. An initial 5 s P1 pulse was applied from the holding potential of −90 mV to potentials between −90 and + 50 mV in 10-mV steps. This was followed immediately by a 1 s P2 depolarization to +50 mV. (*A*) The peak current elicited by the P2 pulse was plotted as a fraction of the maximum value of the peak P1 current. Experiment (□, $n = 5$), and simulations from model C1 (●), model C2 (■), model C3 (▲), and model C4 (▼). (*B*) Simulated current from Model C2 using inset protocol in panel *A*. (*C*) Recovery from inactivation was measured using a standard variable interval gapped pulse protocol. The ratio of the peak current elicited by a 5 s depolarizing pulse from −90 to + 50 mV to the peak current elicited after a variable interval by a second 1 s pulse to + 50 mV was calculated to determine the degree of recovery from inactivation. Data are normalized from the value at time $t = 0$ to 20 s. Experiment (□, $n = 6$) and simulations of model C2 (●) and C2a (■).

models of N-type inactivation occurring only through the open state, or with varying degrees of transitions between the closed and N-type inactivated states:

Model N1

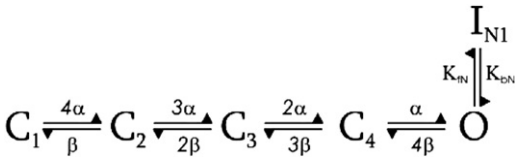

Model N2

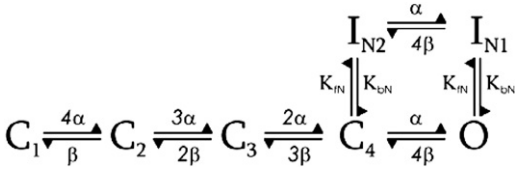

Model N3

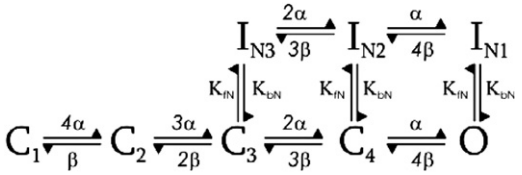

Model N4

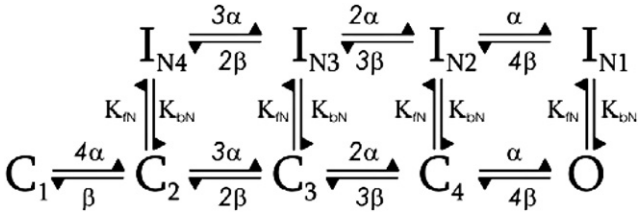

The voltage-independent rate constants into and out of the N-type inactivated state, K_{fN} and K_{bN}, are voltage-insensitive

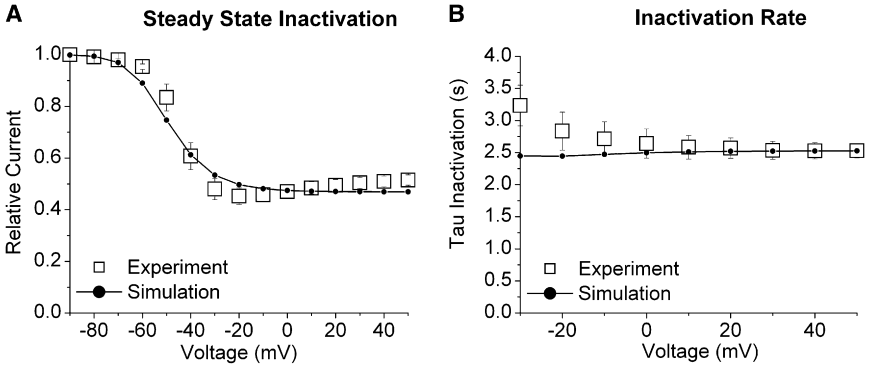

FIGURE 4 The C-type inactivation model C2a coupled to the activation model. (*A*) Isochronal inactivation (compare to Fig. 3 *A*) experiment (□, $n = 5$), and simulations from model C2a (●). (*B*) Rate of C-type inactivation from experiment (□, $n = 7$) and simulation (●).

to reflect the voltage insensitivity of N-terminal binding at positive potentials (11,14). We determined isochronal inactivation in these four models and in experimental data from Kv1.4 and Kv1.4[K532Y] (both with N-terminal intact, i.e., with N- but only limited C-type inactivation). Fig. 5 *A* shows the experimental data were best fit by Model N1, in which the only transition to the N-type inactivated state is from the open state. Fig. 5 *B* shows simulated current using the N1 model of N-type coupled to the activation model, which is equivalent to Kv1.4[K532Y]. This model was used to generate the data shown in Fig. 6. Introduction of N-type inactivation had little effect on the steady-state activation and peak I/V relationships (see the Supporting Material). Inactivation of Kv1.4[K532Y] is well fit by a single exponential, and is voltage-independent at potentials where activation is complete. Similar to C-type inactivation, the transition rates into and out of the N-type inactivated states were therefore modeled as being voltage-independent.

Recovery from N-type inactivation

The recovery of both Kv1.4 and Kv1.4ΔN channels is dominated by the recovery from the C-type inactivated state. Kv1.4[K532Y] channels do not transition easily to the C-type inactivated state, and the few channels which do enter an inactivated state recover from inactivation relatively fast. We compared the recovery from inactivation of Kv1.4 [K532Y] and Model N1, as shown in Fig. 7.

Combined N- and C-type inactivation

Kv1.4 channels exhibit both N- and C-type inactivation, so we combined models C2a and N1 to produce the simplest simulated channel which exhibited both N- and C-type inactivation. The models of N-type and C-type inactivation were combined to produced a Markov model with four closed states, $C_{1\ldots4}$; one open state, O; one N-type inactivated state, I_{N1}; and two C-type inactivated states, I_{C1} and I_{C2}:

Model WT1

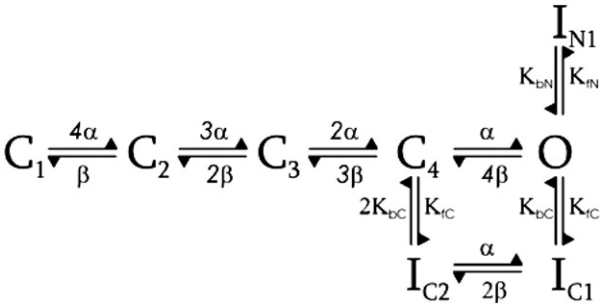

We compared the characteristics of this model against data from wild-type Kv1.4 channels which have both N- and C-type inactivation, as shown in Fig. 8. Merely combining the separate N- and C-type inactivation models does not reproduce the Kv1.4 experimental data. The simulated degree of isochronal inactivation is incomplete, and the simulated recovery from inactivation is much more rapid than observed experimentally.

Coupling between N- and C- type inactivated states

There is significant experimental evidence for coupling between the N-and C-type inactivated states. For example, the rate of development of C-type inactivation is increased in the presence of N-type inactivation (16,17,24). We therefore constructed a model in which the N- and C-type inactivated states were coupled through an N- and C- type inactivated state:

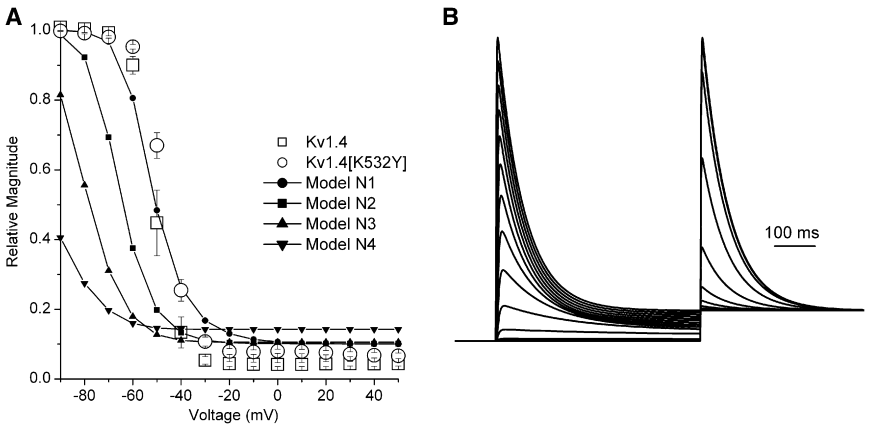

FIGURE 5 Isochronal Inactivation. A 500-ms depolarization (P1) from the holding potential to potentials between −90 and +50 mV was followed by a second 500-ms pulse (P2) to +50 mV. The peak current elicited by P2 was plotted as a fraction of the peak P1 current. (*A*) Experimental data from Kv1.4 (□, $n = 8$), and Kv1.4[K532Y] (○, $n = 8$). Simulations are model N1 (●), N2 (◆), N3 (▲), and N4 (▼). (*B*) Simulated current of Model N1 coupled to the activation model.

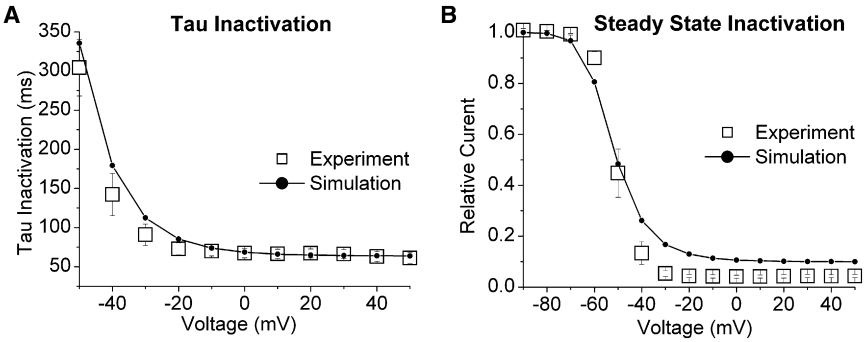

FIGURE 6 Model N1 coupled to the activation model. (*A*) Rate inactivation from experiment (□, $n = 8$) and simulation (●). (*B*) Isochronal inactivation: experiment (□, $n = 8$) simulation (●).

Model WT2

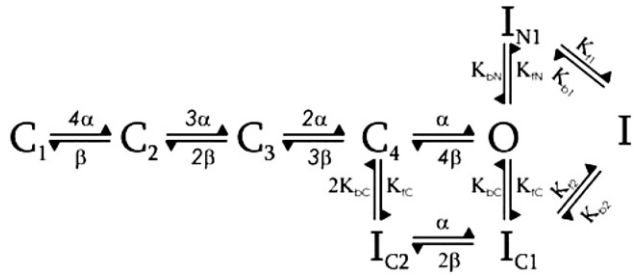

The exact nature of the rates into and out of the combined inactivated state is not necessarily unique. They were constrained to be fast relative to N-type inactivation. If recovery from N-type inactivation is rapid, and recovery from C-type inactivation is slow, comparing the time course of recovery after brief-versus-long depolarization (to favor N- versus C-type, respectively) would show a well-defined transition between fast recovery and slow recovery, but this is not observed experimentally for Kv1.4 (17). In contrast, this is what was observed in *Shaker* (16), which suggests that structural differences in the core domain and/or the N-terminal may influence the nature of this putative transition state.

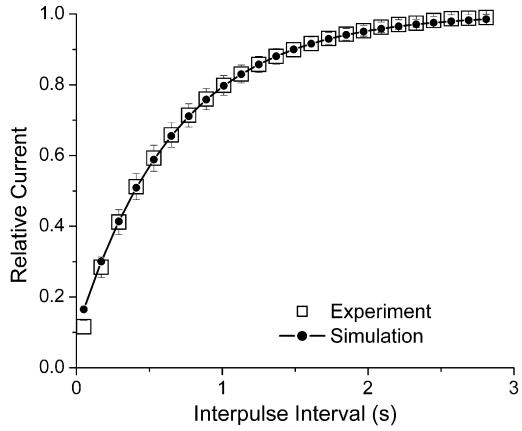

FIGURE 7 Recovery from Inactivation of Kv1.4[K532Y]. A P1 pulse (1 s) was applied from −90 mV to +50 mV. This was followed after a variable interpulse interval by a 1 s P2 pulse to +50 mV. Peak current elicited by P2 was plotted as a fraction of the P1 peak current. Experiment (□, $n = 8$) and simulation (●).

The potential for quantitative differences across closely-related channel types led us to explicitly include this transition state. Mathematically, a direct transition between the states which is consistent with the kinetic data could be derived (25). However, we included a separate state to represent the physical condition where the N-terminal is bound and there is C-type inactivation. This not only accounts for our data, but also allows for more mechanistic modeling applications for situations such as alternative core domains, the presence of ancillary Kvβ subunits which have N-termini (26–28) that can modulate C-type inactivation (19), or open channel pore blocking drugs which promote C-type inactivation such as quinidine (29,30).

Fig. 9 shows that the introduction of a coupled state had small, but important effects on the characteristics of activation. Comparing Fig. 9 *A* to Fig. 2 *D* shows that the coupled model starts to inactivate within the 10-ms depolarizing pulse. However, estimated activation is also marginally faster, and the I/V relationship is well fit. Fig. 9 also shows the inactivation properties of the coupled model. Compared to the uncoupled model, isochronal inactivation is more complete, and recovery from inactivation is slower.

DISCUSSION

Kv1.4 ion channels undergo inactivation via two distinct mechanisms. N-type inactivation is fast, and, when present, dominates channel closure. C-type inactivation is slower,

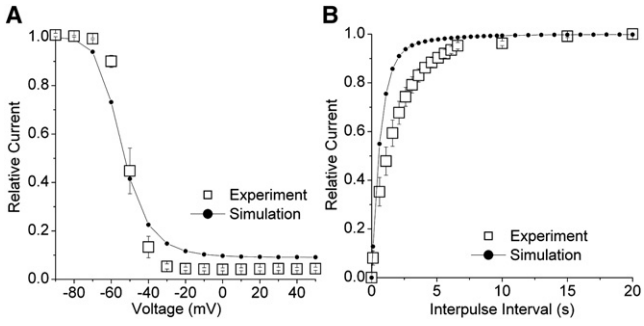

FIGURE 8 Model WT1. (*A*) Isochronal inactivation: experiment (□, $n = 5$) and simulation (●). (*B*) Recovery from inactivation: experiment (□, $n = 5$) and simulation (●).

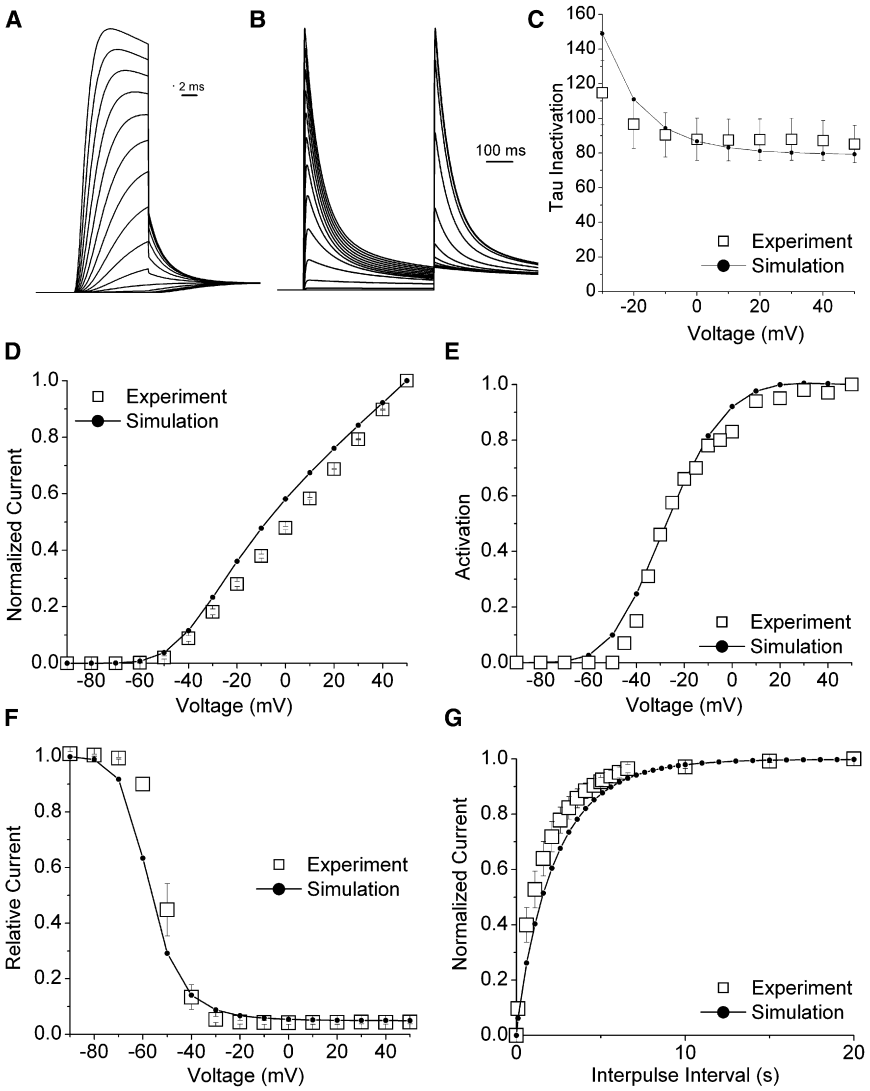

FIGURE 9 Model WT2. (*A*) Simulated current traces showing current activation using the protocol from Fig. 2 *D*. (*B*) Simulated current traces from a two-pulse protocol with P1 (500 ms) to potentials between −90 and +50 mV in 10 mV steps and P2 (500 ms) to +50 mV. (*C*) Rate of inactivation Experiment (□, $n = 5$) and simulation (●). (*D*) Peak-current voltage for experiment (□, $n = 8$) and simulation (●). (*E*) Isochronal activation for experiment (□, from Comer et al. (22)) and simulation (●). (*F*) Isochronal inactivation: experiment (□, $n = 5$) and simulation (●). (*G*) Recovery from inactivation: experiment (□, $n = 5$) and simulation (●).

and is the rate-limiting step controlling the rate of recovery from inactivation. C-type inactivation therefore plays a crucial role in the availability of the channel for the next stimulation in physiological systems. Activation, i.e., channel opening, results in a conformational change of the channel which enables ions to permeate, but also enables the N-terminal region to bind to the intracellular mouth of the pore. In this way Kv1.4 differs from *Shaker*, in which some N-type inactivation may occur from closed states (31).

N-terminal binding occludes the pore, preventing further ion permeation. Occlusion of the conducting pathway by the N-terminal has similarities to intracellular open channel drug block (30). In addition, binding of the N-terminal to the open pore results in conformational changes of both the N-terminal and the pore itself (32). In our model, the channel can only enter the N-type inactivated state from the open state. This is consistent with the molecular basis of N-type inactivation, i.e., binding of the N-terminal to a site that is only accessible when the channel is in the open state.

The mechanisms underlying C-type inactivation are less well defined, but appear to involve significant conformational changes on both the intracellular and extracellular faces of the channel. In the absence of a discrete molecular mechanism, C-type inactivation is defined by a collection of behaviors. C-type inactivation is sensitive to extracellular permeant ions (14,18,20), $[TEA]_o$ (18,33,34), and mutations on the extracellular face of the channel near the mouth of the pore (35,36). In addition, C-type inactivation is affected by intracellular quinidine binding (29,30), intracellular osmotic pressure changes (15), and mutations on the intracellular side of the pore (30,37). C-type inactivation is probably related to the slow inactivation observed in calcium and sodium channels (38–40).

Coupling inactivation to activation

We developed a Markov model of Kv1.4, consisting of four closed states, one open state, two C-type inactivated states,

one N-type inactivated state, and one coupled inactivation state linking the N- and C- type states. Experimental data could only be reproduced adequately by our model when there were direct transitions from the closed state to a C-type inactivated state, as well as coupling between N- and C- type inactivated states. Transitions from a closed state to the inactivated state have been proposed for Kv1.3 channels (41), as well as the more distantly related and more rapidly inactivating Kv4 channels (42,43) and other voltage-gated channels such as *Shaker* Kv1 channels, Kv2.1, Kv3.1, and heteromeric mixtures of Kv channels (44–47). In contrast, N-type inactivation of Kv1.4 appeared to require complete opening of the channel for reproduction of isochronal inactivation in our model analysis.

The exact interpretation of interactions between activation and inactivation in terms of states is somewhat model-dependent, particularly for activation (48). Our base model of activation is derived from a conventional Hodgkin and Huxley (23) analysis of activation, expanded to individual states. This means that the open state is well described in terms of steady-state equilibrium. It does not account, however, for the flickering of the open state (22), and there may be a relatively rapid voltage-insensitive step near the open state, as suggested for the related *Shaker* channel (49). In the Kv1.4 channel, the existence and importance of this is not strongly supported. Castellino et al. (50) (Fig. 4 *H*) used cut-open oocyte clamp to measure the time constant of deactivation down to −150 mV, where it was in the range of 2 ms and had still not shown clear evidence of saturation.

This suggests that, in Kv1.4, a distinct voltage-insensitive C-O step is exceptionally fast, if it exists at all, and that it probably does not contribute in any significant way relative to the development of N-type or C-type inactivation. However, this aspect of activation of Kv1.4 should not be considered conclusively demonstrated. Regardless of the exact model used for activation, the relationship between N-type inactivation and the pseudo-equilibrium of the open state clearly suggest that N-type inactivation is dominated by intracellular pore mouth/gate opening.

The approximation of the activation model to the exact conformational changes associated with the preactivated closed states is clearly an approximation based on voltage dependence, sigmoidicity, and tetrameric structure, and lacks a final voltage-insensitive transition. As such, the activation steps in the model are simple approximations to an undoubtedly more complex overall process. This process involves independent movements of individual voltage sensors (51), cooperative movements involving multiple domains, and a complex process by which the movement of the S4 voltage sensor translates into movement of the intracellular S6 gate and potentially other gates within the channel. Despite the limitations of the simple activation model, it provides a reasonable demonstration of differences in mechanism of N-type and C-type inactivation coupling to activation.

The choice of how to connect inactivated states to activation is also important. The original Hodgkin-Huxley formalism of intrinsic and independent voltage dependence for inactivation is clearly inappropriate for both N- and C-type inactivation. We interpreted this as implying that the transition rates between activated and inactivated states were not functions of membrane potential. The assumption that rates were invariant, regardless of which closed state inactivation was occurring from, was a modeling decision that ultimately was not compatible with our data. The possibility that lower affinity interactions may occur with preactivated states is suggested, but cannot really be considered to be demonstrated on the basis of our analysis and data. However, the experimental data do constrain possible models, particularly in the case of N-type inactivation, where the voltage dependence and completeness of inactivation constrain interactions with preactivated states to be minimal compared with the open state.

The case for C-type inactivation proceeding unequally from all states is less clear. We chose to model C-type inactivation as occurring relatively abruptly once the channel reached a certain level of activation. This abrupt transition from no inactivation to inactivation proceeding at nearly a full rate was meant to reflect the idea that channels near the activated state probably move in a series of large, abrupt conformational transitions (e.g., as evidenced by noise analysis of gating currents (52)). Although our model shows that this type of coupling is consistent with our activation model and inactivation assumptions, the possibility remains that other combinations of parameters for preactivated states and inactivated states may still be possible.

Qualitative observations can be made in a model-independent fashion. The fast development and complete positive isochronal inactivation relationship for N-type intact channels is different from the slower, incomplete development of C-type inactivation, and its more negative isochronal inactivation relationship. Clearly, these qualitative differences demonstrate that C-type inactivation occurs at much more negative potentials and less complete activation than N-type. The development of C-type inactivation therefore behaves as if it occurs without requiring complete opening of the intracellular pore mouth, but may be coupled to preactivated partially open states such as those described by Chapman et al. (53).

Coupling between N-type and C-type inactivation

In addition to coupling to activation, coupling between N- and C- type inactivated states have been proposed (16,30,37). Although N- and C-type inactivation mechanisms are molecularly distinct and are subject to independent manipulation, the two inactivation mechanisms strongly interact. N-type inactivation speeds up the rate at which C-type inactivation occurs (16,17,24). N-type inactivation results from the binding of the N-terminal ball to a binding

site within the open pore. However, the N-terminal and the pore region are both formed from amino acids, and, similar to many protein-protein interactions, N-terminal binding likely results in conformational changes of both the N-terminal and the channel pore. C-type inactivation is sensitive to mutations and manipulations of the pore region (15,30,37,54) and the intracellular gate (15,30), so it is not surprising that N-type inactivation changes the rate of development of C-type inactivation (16–19).

The relationship between N-type inactivation and the rapid development of C-type inactivation are thought to occur via at least two molecular mechanisms, one in which clearance of K^+ from the selectivity filter leads to collapse of the permeation pathway (16,55) and an allosteric mechanism in which C-type inactivation is promoted though large-scale changes in general protein conformation (14,56). Regardless of which mechanism is dominant, it is clear that binding of the N-terminal domain increases the rate of development of C-type inactivation, which in turn dominates recovery of the channel. In this sense, the model state that connects N-type inactivation with C-type inactivation functions as a transition state in which the bound N-terminal domain acts as a catalyst that permits rapid development of the C-type inactivation.

SUPPORTING MATERIAL

Two figures are available at http://www.biophysj.org/biophysj/supplemental/S0006-3495(10)01380-9.

This work was supported in part by the National Institutes of Health (grant Nos. 5R01HL062465 and 5R01HL062465-S1 to R.L.R.), the Oishei Foundation (to R.L.R.), and the American Heart Association (Scientist Development Grant to G.C.L.B.).

REFERENCES

1. Fergus, D. J., J. R. Martens, and S. K. England. 2003. Kv channel subunits that contribute to voltage-gated K^+ current in renal vascular smooth muscle. *Pflugers Arch.* 445:697–704.
2. Trimmer, J. S., and K. J. Rhodes. 2004. Localization of voltage-gated ion channels in mammalian brain. *Annu. Rev. Physiol.* 66:477–519.
3. Veh, R. W., R. Lichtinghagen, …, O. Pongs. 1995. Immunohistochemical localization of five members of the Kv1 channel subunits: contrasting subcellular locations and neuron-specific co-localizations in rat brain. *Eur. J. Neurosci.* 7:2189–2205.
4. Sheng, M., M. L. Tsaur, …, L. Y. Jan. 1992. Subcellular segregation of two A-type K^+ channel proteins in rat central neurons. *Neuron.* 9:271–284.
5. Barry, D. M., and J. M. Nerbonne. 1996. Myocardial potassium channels: electrophysiological and molecular diversity. *Annu. Rev. Physiol.* 58:363–394.
6. Dixon, J. E., and D. McKinnon. 1994. Quantitative analysis of potassium channel mRNA expression in atrial and ventricular muscle of rats. *Circ. Res.* 75:252–260.
7. Tamkun, M. M., K. M. Knoth, …, D. M. Glover. 1991. Molecular cloning and characterization of two voltage-gated K^+ channel cDNAs from human ventricle. *FASEB J.* 5:331–337.
8. Nishiyama, A., D. N. Ishii, …, M. M. Tamkun. 2001. Altered K^+ channel gene expression in diabetic rat ventricle: isoform switching between Kv4.2 and Kv1.4. *Am. J. Physiol. (Heart).* 281:H1800–H1807.
9. Lee, J. K., A. Nishiyama, …, J. Toyama. 1999. Downregulation of voltage-gated K^+ channels in rat heart with right ventricular hypertrophy. *Am. J. Physiol.* 277:H1725–H1731.
10. Kaprielian, R., A. D. Wickenden, …, P. H. Backx. 1999. Relationship between K^+ channel down-regulation and $[Ca^{2+}]_i$ in rat ventricular myocytes following myocardial infarction. *J. Physiol.* 517:229–245.
11. Hoshi, T., W. N. Zagotta, and R. W. Aldrich. 1990. Biophysical and molecular mechanisms of *Shaker* potassium channel inactivation. *Science.* 250:533–538.
12. Zagotta, W. N., T. Hoshi, and R. W. Aldrich. 1990. Restoration of inactivation in mutants of *Shaker* potassium channels by a peptide derived from ShB. *Science.* 250:568–571.
13. Isacoff, E. Y., Y. N. Jan, and L. Y. Jan. 1991. Putative receptor for the cytoplasmic inactivation gate in the *Shaker* K^+ channel. *Nature.* 353:86–90.
14. Rasmusson, R. L., M. J. Morales, …, H. C. Strauss. 1998. Inactivation of voltage-gated cardiac K^+ channels. *Circ. Res.* 82:739–750.
15. Jiang, X., G. C. Bett, …, R. L. Rasmusson. 2003. C-type inactivation involves a significant decrease in the intracellular aqueous pore volume of Kv1.4 K^+ channels expressed in Xenopus oocytes. *J. Physiol.* 549:683–695.
16. Baukrowitz, T., and G. Yellen. 1995. Modulation of K^+ current by frequency and external $[K^+]$: a tale of two inactivation mechanisms. *Neuron.* 15:951–960.
17. Rasmusson, R. L., M. J. Morales, …, H. C. Strauss. 1995. C-type inactivation controls recovery in a fast inactivating cardiac K^+ channel (Kv1.4) expressed in *Xenopus* oocytes. *J. Physiol.* 489:709–721.
18. Hoshi, T., W. N. Zagotta, and R. W. Aldrich. 1991. Two types of inactivation in *Shaker* K^+ channels: effects of alterations in the carboxy-terminal region. *Neuron.* 7:547–556.
19. Morales, M. J., J. O. Wee, …, R. L. Rasmusson. 1996. The N-terminal domain of a K^+ channel β-subunit increases the rate of C-type inactivation from the cytoplasmic side of the channel. *Proc. Natl. Acad. Sci. USA.* 93:15119–15123.
20. Lopez-Barneo, J., T. Hoshi, …, R. W. Aldrich. 1993. Effects of external cations and mutations in the pore region on C-type inactivation of *Shaker* potassium channels. *Receptors Channels.* 1:61–71.
21. Bett, G. C., and R. L. Rasmusson. 2003. Functionally-distinct proton-binding in HERG suggests the presence of two binding sites. *Cell Biochem. Biophys.* 39:183–193.
22. Comer, M. B., D. L. Campbell, …, H. C. Strauss. 1994. Cloning and characterization of an Ito-like potassium channel from ferret ventricle. *Am. J. Physiol.* 267:H1383–H1395.
23. Hodgkin, A. L., and A. F. Huxley. 1952. A quantitative description of membrane current and its application to conduction and excitation in nerve. *J. Physiol.* 117:500–544.
24. Loots, E., and E. Y. Isacoff. 1998. Protein rearrangements underlying slow inactivation of the *Shaker* K^+ channel. *J. Gen. Physiol.* 112: 377–389.
25. Patlak, J. 1991. Molecular kinetics of voltage-dependent Na^+ channels. *Physiol. Rev.* 71:1047–1080.
26. Rettig, J., S. H. Heinemann, …, O. Pongs. 1994. Inactivation properties of voltage-gated K^+ channels altered by presence of β-subunit. *Nature.* 369:289–294.
27. Morales, M. J., R. C. Castellino, …, H. C. Strauss. 1995. A novel β-subunit increases rate of inactivation of specific voltage-gated potassium channel α-subunits. *J. Biol. Chem.* 270:6272–6277.
28. England, S. K., V. N. Uebele, …, M. M. Tamkun. 1995. A novel K^+ channel β-subunit (hKv β 1.3) is produced via alternative mRNA splicing. *J. Biol. Chem.* 270:28531–28534.
29. Wang, S., M. J. Morales, …, R. L. Rasmusson. 2003. Kv1.4 channel block by quinidine: evidence for a drug-induced allosteric effect. *J. Physiol.* 546:387–401.

30. Bett, G. C., and R. L. Rasmusson. 2004. Inactivation and recovery in Kv1.4 K^+ channels: lipophilic interactions at the intracellular mouth of the pore. *J. Physiol.* 556:109–120.

31. Ayer, Jr., R. K., and F. J. Sigworth. 1997. Enhanced closed-state inactivation in a mutant *Shaker* K^+ channel. *J. Membr. Biol.* 157:215–230.

32. Zhou, M., J. H. Morais-Cabral, …, R. MacKinnon. 2001. Potassium channel receptor site for the inactivation gate and quaternary amine inhibitors. *Nature.* 411:657–661.

33. Choi, K. L., R. W. Aldrich, and G. Yellen. 1991. Tetraethylammonium blockade distinguishes two inactivation mechanisms in voltage-activated K^+ channels. *Proc. Natl. Acad. Sci. USA.* 88:5092–5095.

34. Lipkind, G. M., D. A. Hanck, and H. A. Fozzard. 1995. A structural motif for the voltage-gated potassium channel pore. *Proc. Natl. Acad. Sci. USA.* 92:9215–9219.

35. Busch, A. E., R. S. Hurst, …, M. P. Kavanaugh. 1991. Current inactivation involves a histidine residue in the pore of the rat lymphocyte potassium channel RGK5. *Biochem. Biophys. Res. Commun.* 179:1384–1390.

36. Ficker, E., W. Jarolimek, …, A. M. Brown. 1998. Molecular determinants of dofetilide block of HERG K^+ channels. *Circ. Res.* 82: 386–395.

37. Li, X., G. C. Bett, …, R. L. Rasmusson. 2003. Regulation of N- and C-type inactivation of Kv1.4 by pH_o and K^+: evidence for transmembrane communication. *Am. J. Physiol. (Heart).* 284:H71–H80.

38. Qu, Y., J. C. Rogers, …, W. A. Catterall. 1999. Functional roles of the extracellular segments of the sodium channel α-subunit in voltage-dependent gating and modulation by β1 subunits. *J. Biol. Chem.* 274:32647–32654.

39. Zhang, J. F., P. T. Ellinor, …, R. W. Tsien. 1994. Molecular determinants of voltage-dependent inactivation in calcium channels. *Nature.* 372:97–100.

40. Todt, H., S. C. Dudley, Jr., …, H. A. Fozzard. 1999. Ultra-slow inactivation in mu1 Na^+ channels is produced by a structural rearrangement of the outer vestibule. *Biophys. J.* 76:1335–1345.

41. Marom, S., and I. B. Levitan. 1994. State-dependent inactivation of the Kv3 potassium channel. *Biophys. J.* 67:579–589.

42. Wang, S., V. E. Bondarenko, …, H. C. Strauss. 2005. Time- and voltage-dependent components of Kv4.3 inactivation. *Biophys. J.* 89: 3026–3041.

43. Dougherty, K., J. A. Santiago-Castillo, and M. Covarrubias. 2008. Gating charge immobilization in Kv4.2 channels: the basis of closed-state inactivation. *J. Gen. Physiol.* 131:257–273.

44. Klemic, K. G., G. E. Kirsch, and S. W. Jones. 2001. U-type inactivation of Kv3.1 and *Shaker* potassium channels. *Biophys. J.* 81:814–826.

45. Klemic, K. G., C. C. Shieh, …, S. W. Jones. 1998. Inactivation of Kv2.1 potassium channels. *Biophys. J.* 74:1779–1789.

46. Kramer, J. W., M. A. Post, …, G. E. Kirsch. 1998. Modulation of potassium channel gating by coexpression of Kv2.1 with regulatory Kv5.1 or Kv6.1 α-subunits. *Am. J. Physiol.* 274:C1501–C1510.

47. Kerschensteiner, D., and M. Stocker. 1999. Heteromeric assembly of Kv2.1 with Kv9.3: effect on the state dependence of inactivation. *Biophys. J.* 77:248–257.

48. Bett, G. C., and R. L. Rasmusson. 2008. Modification of K^+ channel-drug interactions by ancillary subunits. *J. Physiol.* 586:929–950.

49. Hoshi, T., W. N. Zagotta, and R. W. Aldrich. 1994. *Shaker* potassium channel gating. I: Transitions near the open state. *J. Gen. Physiol.* 103:249–278.

50. Castellino, R. C., M. J. Morales, …, R. L. Rasmusson. 1995. Time- and voltage-dependent modulation of a Kv1.4 channel by a β-subunit (Kv β 3) cloned from ferret ventricle. *Am. J. Physiol.* 269:H385–H391.

51. Bezanilla, F. 2005. Voltage-gated ion channels. *IEEE Trans. Nanobioscience.* 4:34–48.

52. Crouzy, S. C., and F. J. Sigworth. 1993. Fluctuations in ion channel gating currents. Analysis of nonstationary shot noise. *Biophys. J.* 64: 68–76.

53. Chapman, M. L., H. M. VanDongen, and A. M. VanDongen. 1997. Activation-dependent subconductance levels in the Drk1 K channel suggest a subunit basis for ion permeation and gating. *Biophys. J.* 72:708–719.

54. D'Adamo, M. C., Z. Liu, …, M. Pessia. 1998. Episodic ataxia type-1 mutations in the hKv1.1 cytoplasmic pore region alter the gating properties of the channel. *EMBO J.* 17:1200–1207.

55. Gomez-Lagunas, F. 2010. Quinidine interaction with Shab K^+ channels. Pore block and irreversible collapse of the K^+ conductance. *J. Physiol.* 588:2691–2706.

56. Fedida, D., and J. C. Hesketh. 2001. Gating of voltage-dependent potassium channels. *Prog. Biophys. Mol. Biol.* 75:165–199.